

# Collisional Baryon-Dominated Dwarf Galaxies: A New Probe of Bursty Feedback and Dark Matter Physics

Yi-Ying Wang<sup>1</sup>, Daneng Yang<sup>1,2\*</sup>, Keyu Lu<sup>1</sup>, Yue-Lin Sming Tsai<sup>1,2</sup>, Yi-Zhong Fan<sup>1,2\*</sup>

<sup>1</sup>Key Laboratory of Dark Matter and Space Astronomy, Purple Mountain Observatory, Chinese Academy of Sciences, Nanjing 210033, People's Republic of China.

<sup>2</sup>School of Astronomy and Space Science, University of Science and Technology of China, Hefei, Anhui 230026, People's Republic of China.

\*Corresponding author(s). E-mail(s): [yangdn@pmo.ac.cn](mailto:yangdn@pmo.ac.cn); [yzfan@pmo.ac.cn](mailto:yzfan@pmo.ac.cn);

## Abstract

High-velocity collisions between gas-rich ultra-diffuse galaxies present a promising formation channel for baryon-dominated dwarf galaxies (BDDGs). Using hydrodynamical simulations, we show that the progenitors' baryonic binding energy,  $|E_{\text{bind}}|$ , critically controls the outcome. Repeated potential fluctuations, e.g., from bursty feedback, inject energy and reduce  $|E_{\text{bind}}|$  by  $\approx 15\%$ , yielding fewer but substantially more massive BDDGs. By contrast, elastic self-interacting dark matter produces comparable cores without lowering  $|E_{\text{bind}}|$ , resulting in negligible effect. This provides a novel way to distinguish between two leading galactic core formation channels, i.e., the baryon feedback and elastic dark matter self-interaction. Among 15 paired simulation runs, 13 show higher BDDG masses in the weakened-binding case, and about two thirds exhibit  $> 100\%$  mass enhancements. The simulations also predict systematically lower gas fractions due to sustained post-collision star formation, yielding a clean observational signature. Upcoming wide-field imaging (CSST, LSST), HI surveys (FAST), and kinematic follow-up will be crucial to test this scenario.

Within the standard cosmological model, the cosmic baryon fraction is only one-fifth that of the dark matter, and galaxies are expected to reside in more massive dark matter halos. As a result of galaxy formation governed by complex processes, the dark matter content of typical dwarf galaxies is expected to exceed their stellar mass by roughly two orders of magnitude [1–4].

In this context, the observation of galaxies with exceptionally low dark matter content challenges the  $\Lambda$ CDM framework [5–9]. A notable case is NGC 1052-DF2 and DF4 [5, 6], commonly described as dark-matter-deficient galaxies (DMDGs). Both of these are ultra-diffuse systems,

with velocity dispersion measurements consistent with little or no dark matter. Proposed formation scenarios include tidal stripping in cored halos [10–14] and high-velocity collisions that produce dark-matter-deficient remnants [15, 16].

Notably, Guo et al. [7] identified 19 DMDGs from a sample of 324 SDSS dwarfs, with 14 located well beyond the virial radii of nearby groups or clusters, where environmental stripping and recent interactions are unlikely. In a related context, tidal dwarf galaxies (TDGs) are also baryon dominated, forming from the tidal debris of interacting galaxies [17–20]. Kaviraj et al. [19] estimated that about 6% of dwarfs in nearby clusters may have a tidal

origin, while Zaragoza-Cardiel et al. [20] identified 39 TDGs in the local universe that appear to have escaped their host halos. These findings suggest that tidal interactions play a crucial role in producing baryon-dominated galaxies, with galaxy collisions representing the most extreme and favorable conditions for their formation. In this work, we adopt the term baryon-dominated dwarf galaxies (BDDGs) to broadly denote systems in which baryons outweigh dark matter, as expected in collision-driven formation.

In high-speed dwarf–dwarf collisions, ram pressure and shocks can exert forces that separate gas from dark matter, allowing the gas to reassemble into bound, baryon-dominated remnants. Several recent studies have simulated such collisions and demonstrated that gas-rich dwarfs can, under specific conditions, produce remnants with low dark matter content and diffuse morphologies [e.g., 16, 21, 22]. These simulations have examined how collision velocity, disk structure, and initial configuration affect the formation of BDDGs. However, it remains unclear what physical quantity critically controls the mass and yield of BDDGs.

In this work, we identify the baryonic binding energy of the progenitors,  $|E_{\text{bind}}|$ , as the relevant control parameter, directly linking energy injection in dwarf halos to BDDG yields. We employ controlled hydrodynamical simulations of gas-rich ultra-diffuse galaxy (UDG) collisions to assess the potential of these systems as probes of energy injection in dwarf halos, positioning BDDG observations a new observational window for testing the underlying physics. Intriguingly, both baryonic feedback [23–34] and self-interacting dark matter (SIDM) [35–41] have been proposed as mechanisms for generating cores in halos, but their consequences diverge remarkably in collisional events. Future BDDG studies can thus inform both galaxy formation and dark sector physics.

**Weakening gravitational binding by energy injection.** To unbind baryons from halos more efficiently, we need processes that reduce the gravitational binding of the entire system. Although energy injection into halos can weaken the binding of their baryonic component, most baryonic processes, such as gas cooling, release their energy radiatively, thereby dissipating rather than adding energy to the gravitationally bound system. In contrast, repeated potential fluctuations can heat dark matter in the inner regions,

reducing the gravitational binding after relaxation and flattening the inner halo density profile. Such fluctuations arise naturally from bursty stellar feedback in dwarf galaxies [28, 42]. In novel dark matter models, recurrent collapses of solitonic cores can trigger bosenova-like outbursts that drive similar fluctuations [43, 44]. Scattering among dark matter particles may also be exothermic, imparting kinetic energy to the final-state particles while keeping them bound to the halo [45, 46].

As a quantitative illustration, we model the evolution of a halo density profile under energy injection, following the method of Ref. [28], which has been widely applied in various contexts [28, 47–49]. For demonstration, we present results for a spherical, isotropic NFW halo with a mass of  $1.5 \times 10^{10} M_{\odot}$  and a concentration parameter of  $c = 14$ , corresponding to the 1a and 1b benchmarks in Table 1. The baryon content is assumed to be a gas disk which takes spherically averaged pseudo-isothermal profile,  $\rho_{\text{gas}} = \rho_0 (1 + (r/r_g)^2)^{-1}$ , where  $r_g = 2$  kpc and  $\rho_0 = 2.46 \times 10^6 M_{\odot} \text{ kpc}^{-3}$  [16, 50]. The disk height is set to 0.2 kpc.

Figure 1 shows the evolution of the density profile (left), gravitational potential (middle), and  $|E_{\text{bind}}|$  (right) in 2 Gyr. We compute  $E_{\text{bind}}$  by integrating the gas density over the total gravitational potential ( $\Psi_{\text{tot}}$ ),  $E_{\text{bind}} = 4\pi \int dr r^2 \Psi_{\text{tot}} \rho_{\text{gas}}$ . The results illustrate that impulsive feedback heats the inner orbits, leading to an expansion of centrally cored density profile, a shallowing of the central potential, and a reduction in the central baryonic binding energy. By 2 Gyr,  $|E_{\text{bind}}|$  has decreased by over 10%. We will use collision simulations to show that even this modest reduction can substantially enhance the BDDG formation.

We also contrast this with the effect of SIDM, a distinct core formation mechanism. To this end, we simulate the same initial condition as in the 1a and 1b benchmarks (Table 1), considering only gravity and using the `Gadget-2`-based SIDM module developed in Yang et al. [51, 52], adopting a cross section of  $\sigma/m = 20 \text{ cm}^2 \text{ g}^{-1}$ .

In Fig. 1, the evolved density profile at 2 Gyr is shown in gray. While the SIDM halo develops a core of comparable size to that formed by feedback, its gravitational potential remains deep, and  $|E_{\text{bind}}|$  slightly increases rather than decreases.

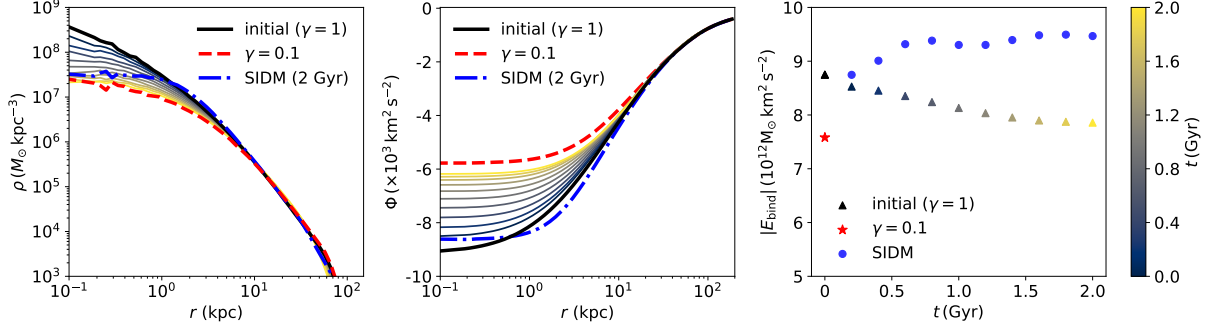


**Fig. 1 Effect of energy injection into dark matter halos.** Repeated potential variations, such as those induced by bursty feedback, can flatten the inner halo densities (left), shallow the potential (middle), and decrease the absolute baryonic binding energy,  $|E_{\text{bind}}|$  (right). The final snapshot resembles a  $\gamma = 0.1$  (red) profile, which features an inner density core and a reduced  $|E_{\text{bind}}|$  relative to the initial cuspy  $\gamma = 1$  profile (black), and we adopt this in our simulations. For comparison, we overlay SIDM results (blue) from a simulation with the same initial  $\gamma = 1$  condition and a cross section per mass  $\sigma/m = 20 \text{ cm}^2/\text{g}$ . The initial conditions correspond to the 1a and 1b benchmarks listed in Table 1.

This suggests that baryonic binding, if quantified observationally, could serve as a diagnostic to distinguish between the two core formation mechanisms.

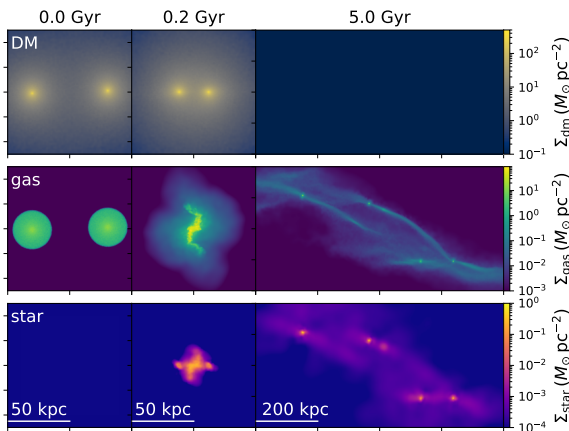


**Fig. 2 Formation of BDDGs from the collision of gas-rich dwarf galaxies.** The initial setup (left) has two progenitors approaching at a close separation. They collide within 0.2 Gyr (middle), displacing gas from the halo centers and triggering efficient star formation. By 5 Gyr (right), the expelled baryons have collapsed into several BDDGs that are far from their progenitors. The surface density distributions of dark matter (top), gas (middle), and stars (bottom) are presented at the corresponding snapshots for the 2a ( $\gamma = 1$ ) benchmark.

**Simulation setup.** To illustrate the impact of energy injection into halos in a model-independent manner, we adopt the following NFW-like extension for the halo density profile [10, 53]

$$\rho(r) = \frac{\rho_s}{\left(\frac{r}{r_s}\right)^\gamma \left(1 + \frac{r}{r_s}\right)^{3-\gamma}}, \quad (1)$$

where the central density slope is governed by  $\gamma$ , with smaller values of  $\gamma$  corresponding to less gravitationally bound halos.

We construct two contrasting sets of initial conditions, one with  $\gamma = 1$  (cuspy) and the other with  $\gamma = 0.1$  (cored, with weaker binding), while keeping the total halo mass and concentration fixed. The simulated halos span masses of  $1 - 2 \times 10^{10} M_\odot$  and concentrations in the range  $4 - 14$ . Assuming these halos host gas-rich UDGs, we model the baryonic content with a gas-only disk, as described previously, and vary the disk height between 0.15 and 0.35 kpc. This maximizes the effectiveness of BDDG formation, as stars behave as a collisionless component during the collision and cannot be efficiently expelled from the progenitors. The gas-to-halo mass ratio is set to 0.1 or 0.22, with gas scale radii  $r_g$  in the range  $1.5 - 3.5$  kpc. These choices are motivated by observations of gas-rich UDGs, where internal turbulence and stellar feedback maintain gas densities below the threshold for molecular hydrogen formation,  $n_g \lesssim$

$1 \text{ cm}^{-3} \approx 3 \times 10^7 M_{\odot} \text{kpc}^{-3}$ , thereby suppressing star formation [42, 54]. The population and properties of gas-rich UDGs have attracted considerable attention and been extensively explored in recent studies [42, 55–59].

Equilibrium initial conditions are generated using DICE [60], with the gas disk stabilized by enforcing a Toomre  $Q_{\text{gas}} > 1.5$  [61, 62]. The gas is initialized at  $T = 10^4 \text{ K}$  and metallicity  $Z = 0.1 Z_{\odot}$ . We evolve the collision simulations using Gadget-4 [63], incorporating radiative cooling of primordial gas and star formation based on the multiphase ISM model of Springel & Hernquist (2003) [64]. Stellar feedback is modeled as an effective pressure that prevents the gas from collapsing too quickly. To obtain the SIDM prediction, we set up a hydrodynamical CDM simulation using progenitors taken from the isolated SIDM simulation (Gadget-2) snapshot at 2 Gyr. We verified that switching off SIDM after this initialization yields a stationary profile in isolation. Further details are provided in the Supplementary Material.

Our collision simulations build upon findings in previous studies, where dependencies of simulation outcomes on the collision velocities, progenitor halo mass and concentration, gas distribution, and numerical resolution were systematically explored. We adopt simulation setups similar to those in Refs. [16, 21, 22], with relative collision velocities ( $v_r$ ) ranging from  $300 - 600 \text{ km/s}$ . Our primary choice of  $v_r = 400 \text{ km/s}$  lies within the preferred range reported in the literature. We also perform simulations with  $v_r = 280, 450$  and  $500 \text{ km/s}$ . The two colliding progenitors are initialized with identical conditions, placed at a separation of  $60 \text{ kpc}$  along their relative velocity vector and with an impact parameter of  $2 \text{ kpc}$ . We focus on contrasting paired samples with  $\gamma = 1$  and  $\gamma = 0.1$ , testing them under a range of conditions. Table 1 summarizes the representative benchmarks adopted in our simulations. Full details of the initial conditions and parameter setup are provided in the Supplementary Material.

**Collisional formation of BDDGs.** Figure 2 shows simulation snapshots of the surface densities of dark matter (top), gas (middle), and stars (bottom) for the benchmark 2a ( $\gamma = 1$ ) in Table 1. Four stages of the collision are displayed. The first snapshot depicts the initial setup, with two progenitors approaching each other at close separation so that the simulation outcome primarily

**Table 1** Representative simulation benchmarks. The full simulation parameters and numerical results are provided in the Supplemental Material.

BM	Profile	$v_r$ (km/s)	$ \frac{\Delta E_{\text{bind}}}{E_{\text{bind}}(\gamma=1)} $	$\frac{M_b(\gamma=0.1)}{M_b(\gamma=1)}$
1a	$\gamma = 1$	400	0.13	7.20
1b	$\gamma = 0.1$	400	0.08	1.83
1c	SIDM	400	0.08	1.83
2a	$\gamma = 1$	400	0.15	5.74
2b	$\gamma = 0.1$	400	0.15	2.53
3a	$\gamma = 1$	280	0.15	2.53
3b	$\gamma = 0.1$	280	0.15	2.53

concerns the formation of BDDGs rather than the internal dynamics of the progenitors. The systems collide within 0.2 Gyr, displacing their gas from the halo centers and triggering efficient star formation. By 5 Gyr, the expelled baryons have already collapsed into several BDDGs and moved far from their progenitors.

With  $v_r = 400 \text{ km/s}$ , most of the progenitor gas is expelled. In the cuspy case ( $\gamma = 1$ ), the steeper dark-matter potential exerts stronger tidal “winds,” causing the expelled gas to fragment into several small, low-mass condensations. In contrast, in the weakened-binding case ( $\gamma = 0.1$ ), the debris remains in contact more easily, allowing it to coalesce into fewer but more massive BDDGs.

To quantify how the tide acts on an extended gas debris, we evaluate on the mid plane the largest eigenvalue ( $\lambda_{\text{max}}$ ) of the tidal tensor  $T \equiv -\nabla \nabla \Phi$ , for which negative eigenvalues imply convergent relative acceleration. Figure 3 shows the head-on collisions between two identical progenitor halos, using parameters from the first benchmark in Table 1, at varying separations:  $d = 0$  (left),  $4$  (middle), and  $8 \text{ kpc}$  (right) for the  $\gamma = 1$  (top),  $\gamma = 0.1$  (middle), and SIDM (bottom) cases. We highlight the  $\lambda_{\text{max}} = 0$  contour, within which all eigenvalues are negative and the tide is compressive.

The  $\gamma = 0.1$  model develops broad, contiguous compressive regions around the origin across all separations, consistent with debris that readily coalesces into fewer, more massive clumps. A shallower inner slope renders the central potential more nearly harmonic, weakens shear, and suppresses stretching along the collision axis. By contrast, the cuspy  $\gamma = 1$  case exhibits only small,

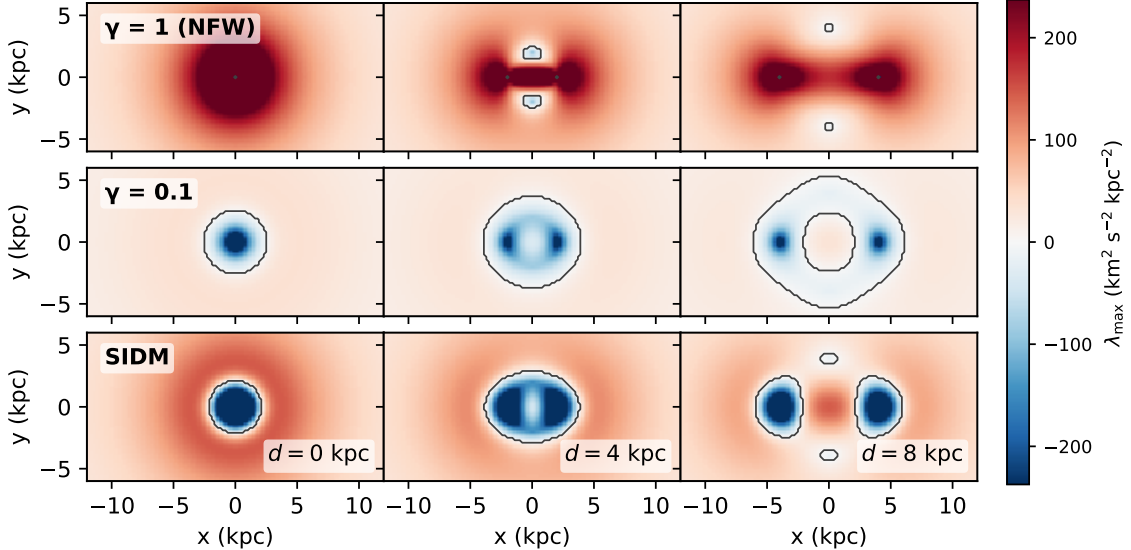


**Fig. 3 Effect of tides on extended gas debris.** The figure shows the largest eigenvalue ( $\lambda_{\max}$ ) of the tidal tensor on the mid-plane for halo pairs with inner slopes of  $\gamma = 1$  (top),  $\gamma = 0.1$  (middle), and a cored SIDM profile (bottom), displayed at separations of  $d = \{0, 4, 8\}$  kpc (columns). Warm colors denote tidal stretching along at least one principal direction ( $\lambda_{\max} > 0$ ), while cold colors indicate fully compressive tides with all eigenvalues negative ( $\lambda_{\max} < 0$ ). The halo parameters follow the first benchmark listed in Table 1.

fragmented compressive islands around shear-dominated zones, consistent with the formation of multiple low-mass condensations. The SIDM core is encircled by a ring of stretching tides that inhibits gas confinement. The central compressive region still facilitates gas condensation, but the formation of BDDG is significantly suppressed compared with the  $\gamma = 0.1$  scenario.

In a weakened gravitational binding scenario, gas is expected to escape more readily during collisions. To illustrate this, we reduce the collision velocity of the 3a and 3b benchmarks to 280 km/s (see Table 1 for setup and results). The escaping gas mass reaches  $3.8 \times 10^9 M_{\odot}$  in the  $\gamma = 0.1$  case, compared to  $3.3 \times 10^9 M_{\odot}$  for  $\gamma = 1$ . Both the stellar and gas masses bound to the resulting BDDGs are substantially higher in the  $\gamma = 0.1$  scenario, with enhancements of 240% and 34%, respectively. The most massive BDDG formed in our simulations has a stellar mass of  $1.68 \times 10^9 M_{\odot}$ , obtained in the  $\gamma = 0.1$ ,  $v_r = 280$  km/s run. These results demonstrate that reduced baryonic binding favors the formation of more massive BDDGs.

Aside from the examples shown, we simulated 15 pairs of dwarf collisions with varied setups. Figure 4 presents the relative BDDG mass enhancements in the  $\gamma = 0.1$  and  $\gamma = 1$  cases,

with bar widths proportional to the reduction in baryonic binding energy and colors indicating the gas fraction,  $f = M_{\text{gas}}/(M_{\text{gas}} + M_{\text{stars}})$ . We find that 13 of the 15 simulations yield an increase in BDDG mass, with 9 of these cases showing an enhancement greater than 100%. The two exceptions occur for halos with extremely low concentrations ( $c = 4$ ) and  $v_r = 450$  km/s, conditions that reduce the contrast between the two scenarios. Interestingly, the gas fractions in the  $\gamma = 0.1$  runs are systematically lower than in their  $\gamma = 1$  counterparts, demonstrating more sustained star formation following the collision. In this figure, we illustrate results considering only the most massive BDDGs. Our findings remain largely unchanged when considering the sum of multiple BDDG masses. The Supplementary Material presents analogous results that include the total BDDG mass as well as the case with the gas cooling rate reduced by half. Additional details on post-collision star formation are also provided.

**Discussion and Conclusion.** Our controlled simulations show that energy injection weakens the progenitors' baryonic binding, elevating BDDG formation through collisions. Repeated potential fluctuations, as expected from bursty stellar feedback, may reduce  $|E_{\text{bind}}|$  by only 15%,

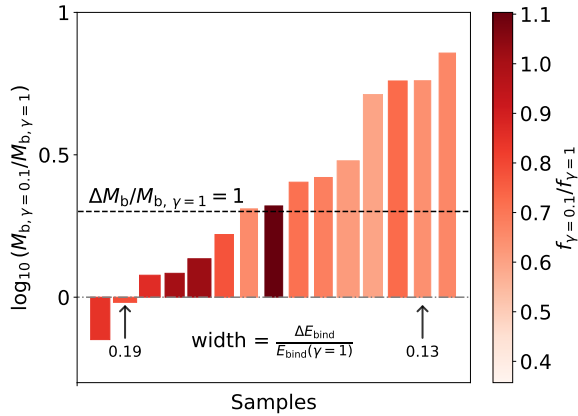


**Fig. 4 Characteristics of the most massive BDDGs in 15 paired simulations.** The bar chart summarizes results from contrasting simulations with inner slopes  $\gamma = 0.1$  and  $\gamma = 1$ . Bars are arranged in ascending order of the BDDG mass ratio,  $M_{b,\gamma=0.1}/M_{b,\gamma=1}$ . The bar width scales with the relative change in binding energy,  $(E_{\text{bind},\gamma=1} - E_{\text{bind},\gamma=0.1})/E_{\text{bind},\gamma=1}$ , while the color indicates the gas fraction,  $f = M_{\text{gas}}/(M_{\text{gas}} + M_{\text{stars}})$ . In contrast, the increase in the BDDG masses is predominantly positive. In 9 out of the 15 simulations, this increase exceeds 100%, as reflected by the bars that rise above the line representing  $\Delta M_b/M_{b,\gamma=1} = 1$ .

yet in two thirds of the simulations, the BDDG masses are enhanced by over 100%. In contrast, SIDM creates cores without lowering  $|E_{\text{bind}}|$  and has a negligible effect on BDDG masses.

Observations of such systems therefore provide a powerful diagnostic of the energy injection mechanisms. Wide-field surveys (LSST, WFST, CSST, Roman, Euclid) will greatly expand catalogs of low-surface-brightness galaxies, identifying BDDG candidates through diffuse morphologies, old stellar populations, and bright globular clusters. However, optical imaging alone cannot confirm their baryon-dominated nature. Crucially, 21-cm surveys (FAST, MeerKAT, VLA) will provide gas fractions and kinematics, establishing whether baryons alone account for the observed dynamical support. Together, these facilities will enable systematic searches, constrain the frequency of BDDG formation, and map their mass spectrum.

Our study focuses on idealized collisions of field galaxies, and analogous processes could also

occur in the collisional formation of TDGs, warranting further investigation. Extending our analysis to cosmological simulations will enable quantification of the BDDG population, determination of the fraction of associated systems, and exploration of the dependence on environment. Aside from energy injection by periodic potential fluctuations, the collisional formation of BDDGs is broadly sensitive to scenarios with weakened gravitational binding. In Warm Dark Matter models, particles possess intrinsically higher initial velocities, leading to shallower inner halo potentials and weaker gravitational binding [65]. Recently, Ref. [49] proposes a model featuring baryon feedback modulated by interactions between baryons and dark matter. Taken together, our results establish BDDG formation as a promising avenue for probing the interplay between feedback-regulated galaxy formation and the fundamental nature of dark matter.

**Acknowledgment.** This work is supported in part by the National Key Research and Development Program of China (No. 2022YFF0503304), the New Cornerstone Science Foundation through the XPLORER PRIZE, the China Manned Space Program (No. CMS-CSST-2025-A03), the Project for Young Scientists in Basic Research of the Chinese Academy of Sciences (No. YSBR-092), the Postdoctoral Fellowship Program of CPSF (No. GZB20250738), and the Jiangsu Funding Program for Excellent Postdoctoral Talent (No. 2025ZB209).

## Appendix A Star formation in gas remnants

Our simulations reveal a systematic trend in which star formation is more efficient when the gravitational binding is weakened. To demonstrate this, we compare the quantity  $b_T$  for the  $\gamma = 1$  (left) and  $\gamma = 0.1$  (right) cases in Fig. A1. This parameter, motivated by the ratio of dynamical to free-fall times, increases with star formation efficiency. Following Ref. [66], we define

$$b_T \equiv \frac{\Sigma_{\text{gas}}}{\sigma_{v,\text{gas}}^2 + c_s^2} \propto \left( \frac{\tau_{\text{dyn}}}{\tau_{\text{ff}}} \right)^2, \quad (\text{A1})$$

with  $c_s = \sqrt{T k_B / (\mu m_p)}$  and  $\mu = 2.3$ .

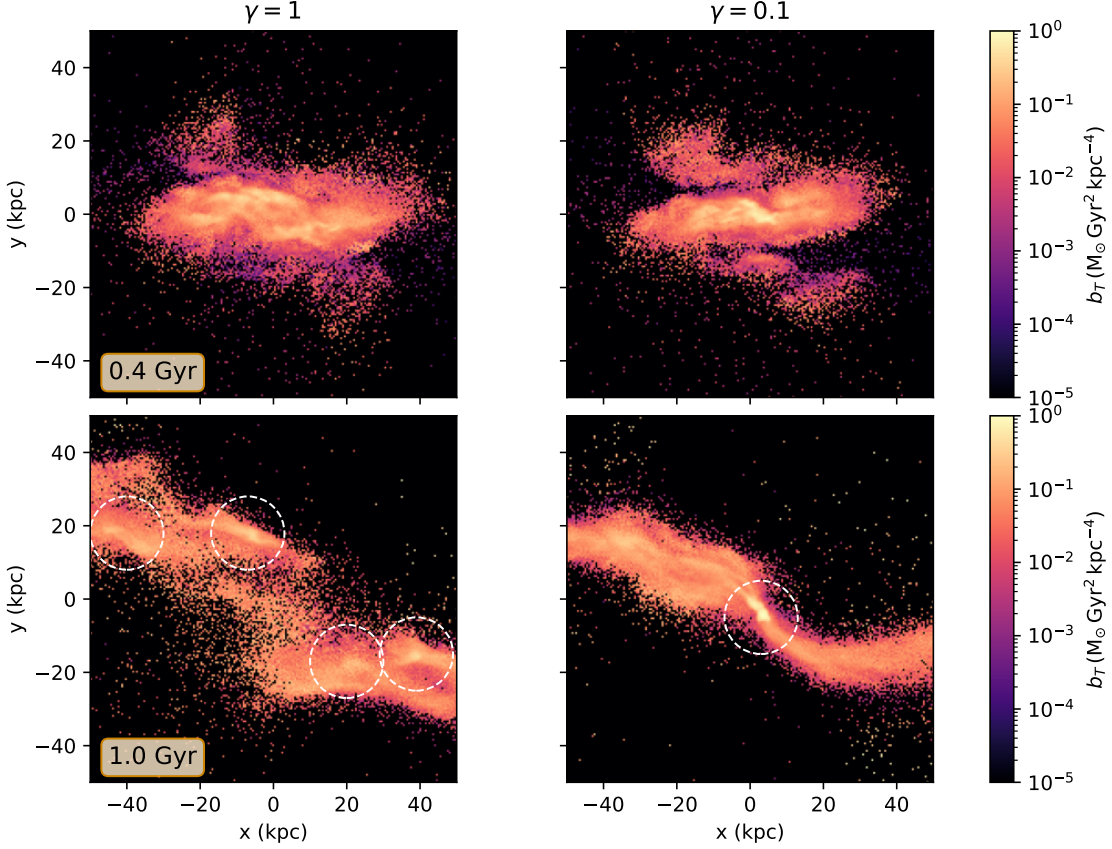


**Fig. A1 Comparison of star formation efficiency in cored and cuspy benchmarks.** Maps of the  $b_T$ , which traces the star formation efficiency, are shown for the cuspy ( $\gamma = 1$ , 2a, left) and cored ( $\gamma = 0.1$ , 2b, right) benchmarks at  $t = 0.4$  Gyr (top) and  $1.0$  Gyr (bottom). White circles mark the sites of the forming BDDGs. The cored ( $\gamma = 0.1$ ) halo develops a significantly brighter region, indicating higher  $b_T$  values and enhanced star formation efficiency at the BDDG site. The cuspy ( $\gamma = 1$ ) halo, while forms four BDDGs, has substantially lower  $b_T$  values.

Figure A1 shows  $b_T$  for the 2a benchmark ( $\gamma = 1$ , left panels) and the 2b benchmark ( $\gamma = 0.1$ , right panels) at  $t = 0.4$  Gyr (top) and  $1.0$  Gyr (bottom). The eventual locations of BDDG formation are enclosed by white circles. In the central collision region, the  $\gamma = 0.1$  case exhibits systematically higher  $b_T$ , corresponding to enhanced star formation. Moreover, in the  $\gamma = 1$  run the gas remnants fragment into three BDDGs, whereas in the  $\gamma = 0.1$  run only a single remnant forms. Similar behavior is observed across multiple paired simulations.

Figure A2 compares the mass evolution of the most massive BDDGs in the 2a ( $\gamma = 1$ ) and 2b

( $\gamma = 0.1$ ) simulations. In the weakened gravitational binding scenario ( $\gamma = 0.1$ ), efficient star formation produces a larger BDDG mass after the collision. Continued star formation beyond 2 Gyr steadily depletes the gas, leading to a decreasing gas fraction. In the  $\gamma = 1$  case, star formation also reduces the gas fraction, but with much lower efficiency, leaving a substantial gas reservoir even at 5 Gyr. In both cases, the total BDDG mass changes only modestly, increasing from  $11 \times 10^8 M_\odot$  ( $2.3 \times 10^8 M_\odot$ ) to  $15 \times 10^8 M_\odot$  ( $2.6 \times 10^8 M_\odot$ ) in the  $\gamma = 0.1$  ( $\gamma = 1$ ) simulation.

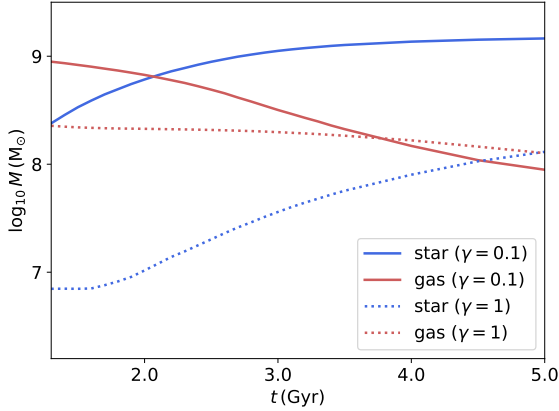


**Fig. A2 Post-collision star formation.** Mass evolution of the most massive BDDGs in the 2a ( $\gamma = 1$ ) and 2b ( $\gamma = 0.1$ ) simulations. In the weakened binding case ( $\gamma = 0.1$ ), efficient star formation yields a more massive BDDG after the collision, with continued activity beyond 2 Gyr steadily depleting the gas reservoir. For  $\gamma = 1$ , star formation is much less efficient, leaving a substantial gas fraction even at 5 Gyr. In both scenarios, the total BDDG mass increases only modestly, from  $11 \times 10^8 M_\odot$  ( $2.3 \times 10^8 M_\odot$ ) to  $15 \times 10^8 M_\odot$  ( $2.6 \times 10^8 M_\odot$ ) in the  $\gamma = 0.1$  ( $\gamma = 1$ ) case.

## Appendix B Stability of SIDM cores

The SIDM benchmark in our study is implemented by incorporating cored halos obtained from a pre-simulation. Specifically, we use `Gadget-2` to evolve an initial system consisting of a gas disk and dark matter under gravity and SIDM ( $\sigma/m = 20 \text{ cm}^2 \text{ g}^{-1}$ ) for 2 Gyr. The final snapshot is then passed to `Gadget-4` to initialize the hydrodynamical collisional simulation. This strategy is justified by the following considerations.

First, radiation pressure in the gaseous disk is subdominant compared to gravitational support; therefore, running the initial SIDM simulation without hydrodynamics does not break the equilibrium of the gas disk, allowing it to be transferred consistently into a subsequent hydrodynamical run. Second, the constant SIDM cross section per mass adopted here should be regarded as an effective constant cross section [67]. In velocity-dependent SIDM models consistent with

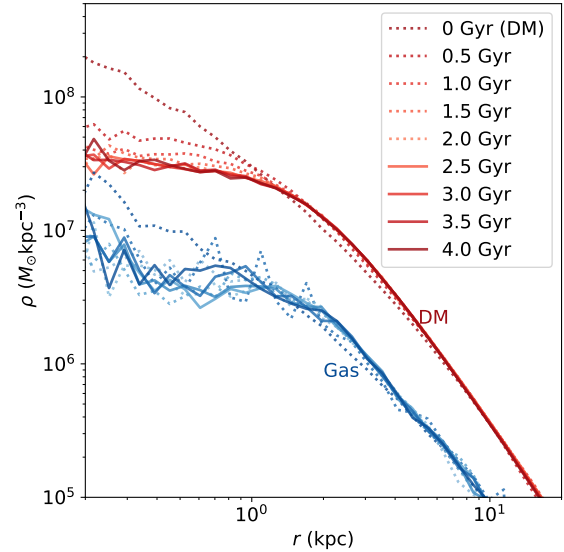


**Fig. B3 Stability test of SIDM halos.** The progenitor system in the 1c simulation is first evolved under SIDM ( $\sigma/m = 20 \text{ cm}^2 \text{ g}^{-1}$ ) for 2 Gyr (dotted lines), when a dark matter core rapidly forms and reaches a stable configuration. SIDM interactions are then turned off and the system is further evolved for 2 Gyr (solid lines). Both the dark matter (red) and stellar (blue) components remain stable, confirming that the SIDM-induced core is long-lived and justifying the neglect of SIDM in the subsequent collisional simulations.

observational constraints, the effect of SIDM during the collision can be neglected because the collision velocity is much larger than the typical particle velocities in the progenitor halos. Lastly, we assume that once SIDM cores form, the resulting cored profiles remain stable over relatively long timescales, even if SIDM interactions are subsequently turned off. This implies that SIDM halos reach a quasi-hydrostatic equilibrium, a point we explicitly verify with a toy simulation.

Figure B3 illustrates this verification for the progenitor system in the 1c simulation. During the first 2 Gyr, the halo evolves under SIDM: the dark matter core develops rapidly within the first  $\sim 1$  Gyr and then approaches a stable configuration. After 2 Gyr, SIDM is switched off and the simulation continues. Both the dark matter (red) and stellar (blue) components remain stable for at least another 2 Gyr. This demonstrates that

neglecting SIDM in the collisional simulation is a valid approximation.

## Appendix C Modeling energy injection into dark matter halos

We model the impact of energy injection into dark matter halos using an analytic framework inspired by Ref. [28]. We initialize a spherical, isotropic NFW halo with mass  $1.5 \times 10^{10} M_\odot$  and concentration  $c = 14$ , corresponding to the 1a and 1b benchmarks in Table 1. For each dark matter particle, we compute the total energy  $E_0$  and specific angular momentum  $j$ . A sequence of impulsive potential fluctuations is modeled by rescaling the potential by a small fraction,  $\Delta V/V_0 = 0.14$ , at each iteration. The energy of each particle is updated using the phase-averaged kick at fixed  $j$

$$\Delta E = \frac{2nE_0}{(2+n)^2} \left( \frac{\Delta V}{V_0} \right)^2, \quad (C2)$$

where  $n = 2$  represents a harmonic oscillator potential. After each impulse, we advance the simulation time by 0.2 Gyr and reconstruct the density profile by summing the orbit-averaged radial probability distributions

$$p(r; E, j) \propto \frac{1}{\sqrt{E - V_{\text{eff}}(r, j)}},$$

$$V_{\text{eff}}(r, j) = V(r) + \frac{j^2}{2r^2},$$

over all dark matter particles.

## Appendix D Tabulated full simulation results

We adopt the gas cooling and star formation module provided in the Gadget-4 code. Radiative cooling is implemented through tabulated rates for primordial gas, while stars form stochastically from dense gas following the multiphase ISM prescription of Springel & Hernquist (2003) [64]. Although our study does not focus on the detailed dynamical processes within UDGs, the efficiency

of gas cooling plays a key role in regulating their stability: a lower cooling rate is generally expected to promote stability. To demonstrate that our conclusions are robust against variations in the cooling rate, we present the full simulation results in Table D1 for the default cooling rate and in Table D2 for a case with the cooling rate reduced by half. In these tables, we identify BDDGs as systems with  $M_*(r < 10\text{kpc}) > 10^6 M_\odot$ , reporting their abundance as well as the mass content of the most massive BDDGs in each simulation.

Figure D4 summarizes the reduced cooling case, in the same format as Fig. 4 in the main text. All key features, most notably the enhancement in BDDG mass and star formation efficiency, remain unaffected. A comparison of the numerical results across the two tables shows that reduced cooling produces more BDDGs with lower characteristic masses. This indicates a potential degeneracy between the effects of gas cooling and weakened gravitational binding. The degeneracy can be resolved by the observed abundance of UDGs, which provides a means to constrain gas cooling [57, 68–70].

Both Fig. 4 and D4 present results for the most massive BDDGs. To further illustrate the robustness of our findings, Fig. D5 shows the total BDDG masses for the default cooling scenario. In all cases, the trend of enhanced BDDG masses in the weakened gravitational binding scenario remains unchanged.

## References

- [1] Dekel, A. & Silk, J. The Origin of Dwarf Galaxies, Cold Dark Matter, and Biased Galaxy Formation. *Astrophys. J.* **303**, 39 (1986).
- [2] Hopkins, P. F. *et al.* Galaxies on FIRE (Feedback In Realistic Environments): Stellar Feedback Explains Cosmologically Inefficient Star Formation. *Mon. Not. Roy. Astron. Soc.* **445**, 581–603 (2014).
- [3] Vale, A. & Ostriker, J. P. Linking halo mass to galaxy luminosity. *Mon. Not. Roy. Astron. Soc.* **353**, 189 (2004).
- [4] Behroozi, P. S., Wechsler, R. H. & Conroy, C. The Average Star Formation Histories of

**Table D1** Galaxy collision simulations with **Gadget-4**: initial collision configurations and properties of the resulting dark-matter-dominated galaxies (DMDGs). The properties listed are: (1) dark matter halo mass  $M_{200}$ , (2) total gas mass, (3) initial relative collision velocity  $v_r$ , (4) gaseous disk scale radius, (5) concentration  $c$ , (6)  $\gamma$ , (7) the absolute value of the baryonic binding energy  $|E_{\text{bind}}|$ , presented in unit  $E_0 \equiv (10^{12} M_{\odot} \text{ km}^2 \text{ s}^{-2})$ , (8) number of resulting DMDGs with  $M_b > 10^6 M_{\odot}$ , (9) stellar mass of the most massive DMDG, and (10) its gas mass. All properties are measured within 10 kpc at  $t = 2.0$  Gyr.

BM	$M_{200, \text{DM}}$ ( $10^{10} M_{\odot}$ )	$M_{\text{gas}}$ ( $10^{10} M_{\odot}$ )	$v_r$ ( $\text{km s}^{-1}$ )	$R_s$ (kpc)	$c$	$\gamma$	$ E_{\text{bind}} $ $E_0$	$n$	$M_{\text{star}}$ ( $10^8 M_{\odot}$ )	$M_{\text{gas}}$ ( $10^8 M_{\odot}$ )
1a	1.5	0.15	400	2	14	1	8.75	1	0.38	1.49
1b						0.1	7.58	1	8.61	4.85
1c	1.5	0.15	400	2	14	SIDM	9.47	1	0.46	2.97
2a	2	0.2	400	2	14	1	14.73	4	0.10	2.13
2b						0.1	12.49	1	6.09	6.72
3a	2	0.2	280	2	14	1	14.73	2	4.89	3.70
3b						0.1	12.49	1	16.80	4.97
4a	1.0	0.1	400	1.5	4	1	3.53	1	0.15	4.13
4b						0.1	2.87	1	0.30	5.54
5a	1.5	0.15	400	2	4	1	7.17	1	6.96	8.32
5b						0.1	5.82	1	9.61	5.05
6a	1.5	0.22	400	2	4	1	10.99	2	16.84	6.02
6b						0.1	9.28	1	20.70	7.03
7a	1.5	0.22	450	2	4	1	10.99	2	2.39	7.74
7b						0.1	9.28	2	3.23	3.96
8a	1.5	0.15	400	2	7	1	7.87	3	1.62	3.38
8b						0.1	6.47	1	11.15	3.91
9a	1.5	0.22	400	2	7	1	11.93	3	4.66	4.42
9b						0.1	10.21	2	18.33	5.57
10a	1.5	0.22	280	2	7	1	11.93	2	12.71	3.15
10b						0.1	10.21	1	25.90	7.27
11a	1.5	0.15	280	2	14	1	8.75	1	0.22	2.14
11b						0.1	7.58	1	8.38	5.20
12a	1.5	0.22	400	2	14	1	13.56	3	3.12	5.88
12b						0.1	11.68	1	13.15	5.23
13a	2	0.2	400	2	4	1	11.72	1	14.64	6.60
13b						0.1	9.75	1	19.49	5.88
14a	2	0.2	400	2	7	1	12.81	2	0.78	3.01
14b						0.1	10.83	1	13.97	5.53
15a	5	0.5	500	3.5	14	1	78.10	3	13.81	4.98
15b						0.1	66.40	1	26.08	5.11

- Galaxies in Dark Matter Halos from  $z = 0\text{--}8$ . *Astrophys. J.* **770**, 57 (2013).
- [5] van Dokkum, P. *et al.* A galaxy lacking dark matter. *Nature* **555**, 629–632 (2018).
- [6] van Dokkum, P., Danieli, S., Abraham, R., Conroy, C. & Romanowsky, A. J. A Second Galaxy Missing Dark Matter in the NGC 1052 Group. *Astrophys. J. Lett.* **874**, L5 (2019).
- [7] Guo, Q. *et al.* Further evidence for a population of dark-matter-deficient dwarf galaxies. *Nature Astron.* **4**, 246–251 (2019).
- [8] Piña Mancera, P. E. *et al.* No need for dark matter: resolved kinematics of the ultra-diffuse galaxy AGC 114905. *Mon. Not. Roy. Astron. Soc.* **512**, 3230–3242 (2022).
- [9] Comerón, S. *et al.* The massive relic galaxy NGC 1277 is dark matter deficient. From

**Table D2** Same as Table D1, but with the cooling rate reduced by half.

BM	$M_{200, \text{DM}}$ ( $10^{10} M_\odot$ )	$M_{\text{gas}}$ ( $10^{10} M_\odot$ )	$v_r$ (km s $^{-1}$ )	$R_s$ (kpc)	$c$	$\gamma$	$ E_{\text{bind}} /E_0 S$	$n$	$M_{\text{star}}$ ( $10^8 M_\odot$ )	$M_{\text{gas}}$ ( $10^8 M_\odot$ )
1a						1	8.75	2	0.02	1.14
1b	1.5	0.15	400	2	14	0.1	7.58	3	0.29	2.35
2a						1	14.73	5	0.02	1.02
2b	2	0.2	400	2	14	0.1	12.49	3	2.08	2.28
3a						1	14.73	4	3.43	2.97
3b	2	0.2	280	2	14	0.1	12.49	2	12.49	4.35
4a						1	3.53	2	0.06	0.55
4b	1.0	0.1	400	1.5	4	0.1	2.87	3	0.15	0.81
5a						1	7.17	2	0.35	2.29
5b	1.5	0.15	400	2	4	0.1	5.82	2	2.33	2.90
6a						1	10.99	1	10.56	7.62
6b	1.5	0.22	400	2	4	0.1	9.28	2	11.29	4.56
8a						1	7.87	2	0.04	0.26
8b	1.5	0.15	400	2	7	0.1	6.47	1	1.64	3.73
9a						1	11.93	3	0.49	2.96
9b	1.5	0.22	400	2	7	0.1	10.21	2	12.68	3.64
10a						1	11.93	2	21.53	5.88
10b	1.5	0.22	280	2	7	0.1	10.21	1	23.94	7.44
11a						1	8.75	2	3.67	2.79
11b	1.5	0.15	280	2	14	0.1	7.58	1	11.84	5.98
12a						1	13.56	4	1.69	3.53
12b	1.5	0.22	400	2	14	0.1	11.68	3	3.72	3.33
13a						1	11.72	3	0.75	3.64
13b	2	0.2	400	2	4	0.1	9.75	1	18.53	1.44
14a						1	12.81	2	0.19	1.91
14b	2	0.2	400	2	7	0.1	10.83	2	7.72	3.42
15a						1	78.10	5	16.31	4.45
15b	5	0.5	500	3.5	14	0.1	66.40	4	23.62	4.14

- dynamical models of integral-field stellar kinematics out to five effective radii. *Astron. Astrophys.* **675**, A143 (2023).
- [10] Ogiya, G. Tidal stripping as a possible origin of the ultra diffuse galaxy lacking dark matter. *Mon. Not. R. Astron. Soc.* **480**, L106–L110 (2018).
- [11] Yang, D., Yu, H.-B. & An, H. Self-Interacting Dark Matter and the Origin of Ultradiffuse Galaxies NGC1052-DF2 and -DF4. *Phys. Rev. Lett.* **125**, 111105 (2020).
- [12] Sales, L. V. *et al.* The formation of ultradiffuse galaxies in clusters. *Mon. Not. R. Astron. Soc.* **494**, 1848–1858 (2020).
- [13] Zhang, Z.-C., Bi, X.-J. & Yin, P.-F. Tidal Formation of Dark Matter Deficit Diffuse Galaxy NGC 1052-DF2 by SIDM. *Astrophys. J.* **981**, 89 (2025).
- [14] Zhang, Z.-C., Bi, X.-J. & Yin, P.-F. Reproduction of NGC1052-DF4 by self-interacting dark matter: dark matter deficiency and tidal features. *JCAP* **03**, 031 (2025).
- [15] van Dokkum, P. *et al.* A trail of dark-matter-free galaxies from a bullet-dwarf collision. *Nature* **605**, 435–439 (2022).
- [16] Lee, J., Shin, E.-j., Kim, J.-h., Shapiro, P. R. & Chung, E. Multiple Beads on a String: Dark-matter-deficient Galaxy Formation in a

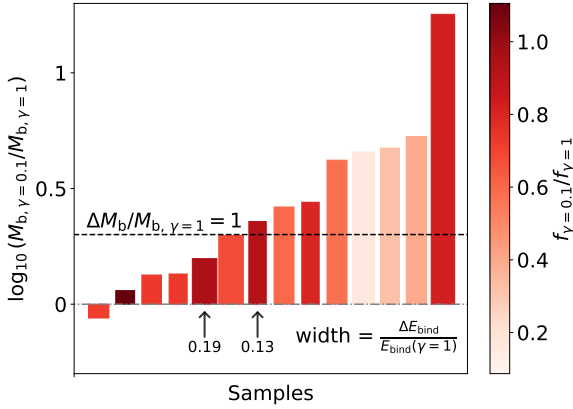


**Fig. D4 Characteristics of the most massive BDDGs in 14 paired simulations with reduced gas cooling.** The bar chart summarizes results from contrasting simulations with inner slopes  $\gamma = 0.1$  and  $\gamma = 1$ . Bars are arranged in ascending order of the BDDG mass ratio,  $M_{b,\gamma=0.1}/M_{b,\gamma=1}$ . The bar width scales with the relative change in binding energy,  $(E_{\text{bind},\gamma=1} - E_{\text{bind},\gamma=0.1})/E_{\text{bind},\gamma=1}$ , while the color indicates the gas fraction,  $f = M_{\text{gas}}/(M_{\text{gas}} + M_{\text{stars}})$ . In contrast, the increase in the BDDG masses is predominantly positive. In 8 out of the 15 simulations, this increase exceeds 100%, as reflected by the bars that rise above the line representing  $\Delta M_b/M_{b,\gamma=1} = 1$ .

Mini-Bullet Satellite–Satellite Galaxy Collision. *Astrophys. J.* **966**, 72 (2024).

- [17] Bournaud, F. & Duc, P. A. From Tidal Dwarf Galaxies to Satellite Galaxies. *Astron. Astrophys.* **456**, 481 (2006).
- [18] Gentile, G. *et al.* Tidal dwarf galaxies as a test of fundamental physics. *Astron. Astrophys.* **472**, L25 (2007).
- [19] Kaviraj, S., Darg, D., Lintott, C., Schawinski, K. & Silk, J. Tidal dwarf galaxies in the nearby Universe. *Mon. Not. R. Astron. Soc.* **419**, 70–79 (2012).
- [20] Zaragoza-Cardiel, J. *et al.* Detection and characterization of detached tidal dwarf galaxies. *Astron. Astrophys.* **689**, A206 (2024).
- [21] Shin, E.-j. *et al.* Dark Matter Deficient Galaxies Produced via High-velocity Galaxy

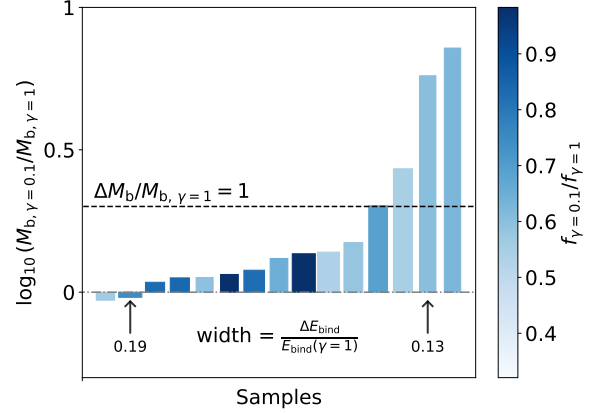


**Fig. D5 Characteristics of the summed BDDG content for 15 paired simulations.** The bar chart summarizes results from contrasting simulations with inner slopes  $\gamma = 0.1$  and  $\gamma = 1$ . Bars are arranged in ascending order of the summed BDDG mass ratio,  $M_{b,\gamma=0.1}/M_{b,\gamma=1}$ . The bar width scales with the relative change in binding energy,  $(E_{\text{bind},\gamma=1} - E_{\text{bind},\gamma=0.1})/E_{\text{bind},\gamma=1}$ , while the color indicates the gas fraction,  $f = M_{\text{gas}}/(M_{\text{gas}} + M_{\text{stars}})$ . In contrast, the increase in the BDDG masses is predominantly positive. In 4 out of the 15 simulations, this increase exceeds 100%, as reflected by the bars that rise above the line representing  $\Delta M_b/M_{b,\gamma=1} = 1$ .

Collisions in High-resolution Numerical Simulations. *Astrophys. J.* **899**, 25 (2020).

- [22] Lee, J., Shin, E.-j. & Kim, J.-h. Dark Matter Deficient Galaxies and Their Member Star Clusters Form Simultaneously during High-velocity Galaxy Collisions in 1.25 pc Resolution Simulations. *Astrophys. J. Lett.* **917**, L15 (2021).
- [23] Navarro, J. F., Eke, V. R. & Frenk, C. S. The cores of dwarf galaxy halos. *Mon. Not. Roy. Astron. Soc.* **283**, L72–L78 (1996).
- [24] Gnedin, O. Y. & Zhao, H. Maximum feedback and dark matter profiles of dwarf galaxies. *Mon. Not. Roy. Astron. Soc.* **333**, 299 (2002).
- [25] Read, J. I. & Gilmore, G. Mass loss from dwarf spheroidal galaxies: The Origins of shallow dark matter cores and exponential surface brightness profiles. *Mon. Not. Roy. Astron. Soc.* **356**, 107–124 (2005).

- [26] Mashchenko, S., Couchman, H. M. P. & Wadsley, J. The removal of cusps from galaxy centres by stellar feedback in the early Universe. *Nature* **442**, 539–542 (2006).
- [27] Governato, F. *et al.* Bulgeless dwarf galaxies and dark matter cores from supernova-driven outflows. *Nature* **463**, 203–206 (2010).
- [28] Pontzen, A. & Governato, F. How supernova feedback turns dark matter cusps into cores. *Mon. Not. R. Astron. Soc.* **421**, 3464–3471 (2012).
- [29] Ogiya, G. & Mori, M. The core-cusp problem in cold dark matter halos and supernova feedback: Effects of Oscillation. *Astrophys. J.* **793**, 46 (2014).
- [30] Chan, T. K. *et al.* The impact of baryonic physics on the structure of dark matter haloes: the view from the FIRE cosmological simulations. *Mon. Not. Roy. Astron. Soc.* **454**, 2981–3001 (2015).
- [31] Tollet, E. *et al.* NIHAO - IV: core creation and destruction in dark matter density profiles across cosmic time. *Mon. Not. R. Astron. Soc.* **456**, 3542–3552 (2016).
- [32] Salucci, P. The distribution of dark matter in galaxies. *Astron. Astrophys. Rev.* **27**, 2 (2019).
- [33] Lazar, A. *et al.* A dark matter profile to model diverse feedback-induced core sizes of  $\Lambda$ CDM haloes. *Mon. Not. R. Astron. Soc.* **497**, 2393–2417 (2020).
- [34] Macciò, A. V., Crespi, S., Blank, M. & Kang, X. NIHAO – XXIII. Dark matter density shaped by black hole feedback. *Mon. Not. Roy. Astron. Soc.* **495**, L46–L50 (2020).
- [35] Spergel, D. N. & Steinhardt, P. J. Observational evidence for selfinteracting cold dark matter. *Phys. Rev. Lett.* **84**, 3760–3763 (2000).
- [36] Tulin, S. & Yu, H.-B. Dark matter self-interactions and small scale structure. *Physics Reports* **730**, 1–57 (2018).
- [37] Adhikari, S. *et al.* Astrophysical Tests of Dark Matter Self-Interactions (2022).
- [38] Kochanek, C. S. & White, M. J. A Quantitative study of interacting dark matter in halos. *Astrophys. J.* **543**, 514 (2000).
- [39] Vogelsberger, M., Zavala, J. & Loeb, A. Subhaloes in self-interacting galactic dark matter haloes. *Mon. Not. R. Astron. Soc.* **423**, 3740–3752 (2012).
- [40] Kaplinghat, M., Tulin, S. & Yu, H.-B. Dark Matter Halos as Particle Colliders: Unified Solution to Small-Scale Structure Puzzles from Dwarfs to Clusters. *Phys. Rev. Lett.* **116**, 041302 (2016).
- [41] Zhang, Z. *et al.* Unexpected clustering pattern in dwarf galaxies challenges formation models. *Nature* **642**, 47–52 (2025).
- [42] Chan, T. K. *et al.* The origin of ultra diffuse galaxies: stellar feedback and quenching. *Mon. Not. R. Astron. Soc.* **478**, 906–925 (2018).
- [43] Fox, P. J., Weiner, N. & Xiao, H. Recurrent axion stars collapse with dark radiation emission and their cosmological constraints. *Phys. Rev. D* **108**, 095043 (2023).
- [44] Koo, H. Head-on collisions of fuzzy/cold dark matter subhalos. *J. Korean Phys. Soc.* **87**, 430–440 (2025).
- [45] Vogelsberger, M., Zavala, J., Schutz, K. & Slatyer, T. R. Evaporating the Milky Way halo and its satellites with inelastic self-interacting dark matter. *Mon. Not. Roy. Astron. Soc.* **484**, 5437–5452 (2019).
- [46] Medvedev, M. V. Cosmological Simulations of Multicomponent Cold Dark Matter. *Phys. Rev. Lett.* **113**, 071303 (2014).
- [47] Di Cintio, A. *et al.* The dependence of dark matter profiles on the stellar-to-halo mass ratio: a prediction for cusps versus cores. *Mon. Not. R. Astron. Soc.* **437**, 415–423 (2014).

- [48] Peirani, S. *et al.* Density profile of dark matter haloes and galaxies in the HORIZON-AGN simulation: the impact of AGN feedback. *Mon. Not. R. Astron. Soc.* **472**, 2153–2169 (2017).
- [49] Acevedo, J. F. *et al.* Dark matter induced baryonic feedback in galaxies. *Phys. Rev. D* **110**, 083004 (2024).
- [50] Kurapati, S., Chengalur, J. N., Kamphuis, P. & Pustilnik, S. Mass models of gas-rich void dwarf galaxies. *Mon. Not. R. Astron. Soc.* **491**, 4993–5014 (2020).
- [51] Yang, D. & Yu, H.-B. Gravothermal evolution of dark matter halos with differential elastic scattering. *J. Cosmol. Astropart. Phys.* **2022**, 077 (2022).
- [52] Yang, D., Nadler, E. O. & Yu, H.-B. Strong Dark Matter Self-interactions Diversify Halo Populations within and surrounding the Milky Way. *Astrophys. J.* **949**, 67 (2023).
- [53] Graham, A. W., Merritt, D., Moore, B., Diemand, J. & Terzic, B. Empirical models for Dark Matter Halos. I. Nonparametric Construction of Density Profiles and Comparison with Parametric Models. *Astron. J.* **132**, 2685–2700 (2006).
- [54] Di Cintio, A. *et al.* NIHAO – XI. Formation of ultra-diffuse galaxies by outflows. *Mon. Not. Roy. Astron. Soc.* **466**, L1–L6 (2017).
- [55] Papastergis, E., Adams, E. A. K. & Romanowsky, A. J. The HI content of isolated ultra-diffuse galaxies: A sign of multiple formation mechanisms? *Astron. Astrophys.* **601**, L10 (2017).
- [56] Jiang, F. *et al.* Formation of ultra-diffuse galaxies in the field and in galaxy groups. *Mon. Not. Roy. Astron. Soc.* **487**, 5272–5290 (2019).
- [57] Jones, M. G. *et al.* Contribution of HI-bearing ultra-diffuse galaxies to the cosmic number density of galaxies. *Astron. Astrophys.* **614**, A21 (2018).
- [58] Mancera Piña, P. E. *et al.* Robust HI kinematics of gas-rich ultra-diffuse galaxies: hints of a weak-feedback formation scenario. *Mon. Not. Roy. Astron. Soc.* **495**, 3636–3655 (2020).
- [59] Kong, D., Kaplinghat, M., Yu, H.-B., Fraternali, F. & Mancera Piña, P. E. The Odd Dark Matter Halos of Isolated Gas-rich Ultradiffuse Galaxies. *Astrophys. J.* **936**, 166 (2022).
- [60] Perret, V. *et al.* Evolution of the mass, size, and star formation rate in high redshift merging galaxies. MIRAGE - A new sample of simulations with detailed stellar feedback. *Astron. Astrophys.* **562**, A1 (2014).
- [61] Toomre, A. On the gravitational stability of a disk of stars. *Astrophys. J.* **139**, 1217–1238 (1964).
- [62] Binney, J. & Tremaine, S. *Galactic Dynamics: Second Edition* (2008).
- [63] Springel, V., Pakmor, R., Zier, O. & Reincke, M. Simulating cosmic structure formation with the GADGET-4 code. *Mon. Not. R. Astron. Soc.* **506**, 2871–2949 (2021).
- [64] Springel, V. & Hernquist, L. Cosmological SPH simulations: A Hybrid multi-phase model for star formation. *Mon. Not. Roy. Astron. Soc.* **339**, 289 (2003).
- [65] Gilman, D. *et al.* Warm dark matter chills out: constraints on the halo mass function and the free-streaming length of dark matter with eight quadruple-image strong gravitational lenses. *Mon. Not. Roy. Astron. Soc.* **491**, 6077–6101 (2020).
- [66] Leroy, A. K. *et al.* A Portrait of Cold Gas in Galaxies at 60 pc Resolution and a Simple Method to Test Hypotheses That Link Small-scale ISM Structure to Galaxy-scale Processes. *Astrophys. J.* **831**, 16 (2016).
- [67] Yang, D. & Yu, H.-B. Gravothermal evolution of dark matter halos with differential elastic scattering. *JCAP* **09**, 077 (2022).

- [68] Rong, Y. *et al.* A Universe of ultradiffuse galaxies: theoretical predictions from  $\Lambda$ CDM simulations. *Mon. Not. R. Astron. Soc.* **470**, 4231–4240 (2017).
- [69] van der Burg, R. F. J. *et al.* The abundance of ultra-diffuse galaxies from groups to clusters. UDGs are relatively more common in more massive haloes. *Astron. Astrophys.* **607**, A79 (2017).
- [70] Di Cintio, A. *et al.* NIHAO - XI. Formation of ultra-diffuse galaxies by outflows. *Mon. Not. R. Astron. Soc.* **466**, L1–L6 (2017).